IOPscience iopscience.iop.org

Home Search Collections Journals About Contact us My IOPscience

First-principles study of vacancy formation in $LaNi_5$

This article has been downloaded from IOPscience. Please scroll down to see the full text article.

2008 J. Phys.: Condens. Matter 20 275232

(http://iopscience.iop.org/0953-8984/20/27/275232)

View the table of contents for this issue, or go to the journal homepage for more

Download details:
IP Address: 129.252.86.83
The article was downloaded on 29/05/2010 at 13:25

Please note that terms and conditions apply.

J. Phys.: Condens. Matter **20** (2008) 275232 (5pp) doi:10.1088/0953-8984/20/27/275232

First-principles study of vacancy formation in $LaNi_5$

Masataka Mizuno, Hideki Araki and Yasuharu Shirai

Center for Atomic and Molecular Technologies, Graduate School of Engineering, Osaka University, 2-1 Yamadaoka, Suita, Osaka 565-0871, Japan

E-mail: mizuno@mat.eng.osaka-u.ac.jp

Received 4 April 2008, in final form 13 May 2008
Published 6 June 2008
Online at stacks.iop.org/JPhysCM/20/275232

Abstract

First-principles electronic structure calculations have been performed in order to investigate vacancy formation in $LaNi_5$. The Ni dumbbells at La sites accommodate the excess Ni atoms removed as Ni vacancies. Clear site dependence is observed in vacancy formation energies: the formation energy of the Ni vacancy at the 2c site is about 0.8 eV lower than that at the 3g site. The formation of Ni vacancies at the 2c sites leads to the decrease of the lattice parameter a and the increase of the lattice parameter c. This trend shows good agreement with the change in lattice parameters by activation of $LaNi_5$. Our calculated results indicate that Ni vacancies are mainly formed at the 2c sites in the hydrogen absorption–desorption process in $LaNi_5$.

1. Introduction

The intermetallic compound $LaNi_5$ possesses exceptional properties that make it suitable as a hydrogen storage material. The hydrogen absorption process is accompanied by a large volume expansion, which causes the formation of lattice defects. Our positron lifetime measurement revealed that not only dislocations but also vacancies and vacancy clusters are formed in the hydrogen absorption–desorption process in $LaNi_5$ [1, 2]. We also investigated lattice defects in $LaNi_5$ using theoretical calculations of positron lifetimes to find that vacancy clusters formed in the hydrogen absorption–desorption process are composed of Ni vacancies [3, 4]. On the other hand, it is well known that a loss of hydrogen storage capacity occurs during absorption–desorption cycles in $LaNi_5$. Substituted $LaNi_5$ alloys have been investigated for modifications of hydrogenation properties. In particular, substitution of Sn for Ni in $LaNi_5$ remarkably reduces the degree of degradation [5]. Our recent study using positron lifetime measurement indicates that the increase in mean positron lifetime during hydrogen absorption–desorption cycling for $LaNi_{4.8}Sn_{0.2}$ is less than that for $LaNi_5$; that is, the formation of vacancies during the cycling is reduced by the addition of Sn [6]. This result suggests that the addition of Sn affects the stability of vacancies. Understanding vacancy formation can play an important role in reducing the loss of hydrogen storage capacity. In ordered compounds, the process of vacancy formation is more complicated than in monoatomic crystals because more than one type of defect must be created simultaneously in order to conserve the homogeneity of the sample. However, to our knowledge, there have been no reports on the nature of vacancies in $LaNi_5$. Whereas our final goal is to study the effect of hydrogen and additional elements on vacancy formation in $LaNi_5$ using theoretical calculations, we have to clarify the process of vacancy formation in pure $LaNi_5$.

In the present work, we have performed first-principles electronic structure calculations in order to evaluate vacancy formation energies and vacancy-induced change in lattice parameters in $LaNi_5$. Constitutional defects formed in non-stoichiometric $LaNi_5$ are also determined to obtain the chemical potential of the constituent atoms of $LaNi_5$. The calculated lattice parameters including vacancies are compared with experimental results.

2. Computational method

We employed the Vienna *ab initio* simulation package (VASP) [7, 8] with the generalized gradient approximation proposed by Perdew and Wang [9]. Potentials based upon the all-electron projector augmented wave (PAW) method were used [10, 11]. The intermetallic compound $LaNi_5$ crystallizes in the hexagonal $CaCu_5$ type structure, which belongs to the space group $P6/mmm$ with lattice parameters of $a = 5.0228$ Å and $c = 3.9826$ Å [12], as shown in figure 1. First, we calculated the equilibrium lattice parameters of $LaNi_5$ using the kinetic energy cut-off of 350 eV and a $15 \times 15 \times 19$ k-mesh

 © 2008 IOP Publishing Ltd Printed in the UK

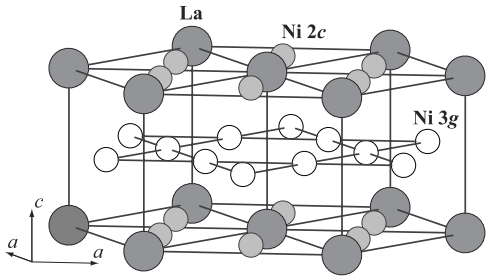

Figure 1. Crystal structure of $LaNi_5$.

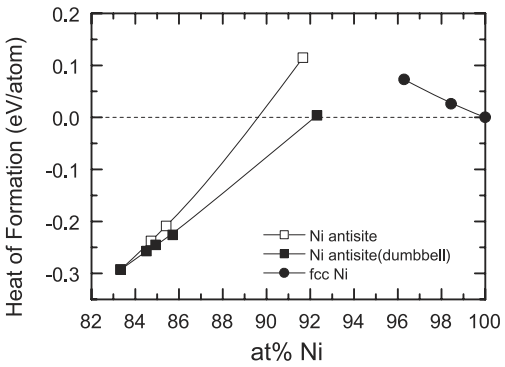

Figure 2. Heat of formation of the La–Ni system around $LaNi_5$ as a function of Ni composition.

in the Monkhorst–Pack scheme with the unit cell including six atoms. We obtained the equilibrium lattice parameter of $a = 5.0107$ Å and $c = 3.9690$ Å, which well reproduce the experimental values. The structure of $LaNi_5$ consists of stacking of two types of layers: one is composed of La atoms at the 1a sites and Ni atoms at the 2c sites, the other is composed of Ni atoms on the 3g sites. Our results using positron lifetime measurements and theoretical calculations ruled out the possibility of the formation of La vacancies during hydrogen absorption [3, 4]. Ni vacancies at the 2c and 3g sites are, therefore, considered in the present work.

The formation energy of a Ni vacancy, E_V^{Ni}, can be calculated using the defect energy parameter, $\varepsilon_V^{\mathrm{Ni}}$, and the chemical potential, μ_{Ni} [13]:

$$E_V^{\mathrm{Ni}} = \varepsilon_V^{\mathrm{Ni}} + \mu_{\mathrm{Ni}}. \tag{1}$$

The defect energy parameter is defined as the energy difference between the supercell including a defect and the ideal supercell of N atoms:

$$\varepsilon_V^{\mathrm{Ni}} = E(N_{\mathrm{La}}, N_{\mathrm{Ni}} - 1, V^{\mathrm{Ni}}) - E(N_{\mathrm{La}}, N_{\mathrm{Ni}}, 0). \tag{2}$$

Here $E(N_{\mathrm{La}}, N_{\mathrm{Ni}} - 1, V^{\mathrm{Ni}})$ denotes the energy of a supercell with $N_{\mathrm{La}} + N_{\mathrm{Ni}} - 1$ atoms including one Ni vacancy. In the present work, we employed the $2 \times 2 \times 4$ supercells composed of 16 La and 80 Ni lattice sites to calculate the defect energy parameters. Relaxations of the atomic positions and lattice parameters were allowed.

The chemical potential is used for the compensation of the energy of atoms related to defect formation. The chemical potential of the Ni atom removed as a Ni vacancy is supposed to be that of metal Ni at room temperature because the compositional range around the stoichiometric composition of $LaNi_5$ nearly vanishes around 1273 K and the adjacent phase in the Ni-rich side of $LaNi_5$ is fcc Ni. On the other hand, vacancy migration in $LaNi_5$ after hydrogen desorption at 296 K is observed around 427–673 K [2]. Room temperature is not, therefore, high enough for metal Ni to precipitate. In $LaNi_{5+x}$ annealed at 1473 K La atoms are partially substituted not by Ni atoms but by Ni dumbbells (two Ni atoms) [14, 15]. In the present work, the energy of a Ni atom both in fcc Ni and in a Ni dumbbell at the La site are considered as the chemical potential of the Ni atom. The chemical potential of a Ni atom in metal Ni is obtained from the energy of fcc Ni. In the case of the Ni dumbbell, conserving the alloy composition needs to be taken into account. One La atom removed for the formation of a Ni dumbbell requires extra La + 5Ni sites. One Ni dumbbell, therefore, accommodates seven Ni atoms (two Ni atoms as a Ni dumbbell and five Ni atoms at extra La + 5Ni sites). The formation of Ni vacancies and Ni dumbbells proceeds via the reaction

$$0 \rightarrow V_{\mathrm{Ni}} + \tfrac{1}{7}(\mathrm{Ni}_{\mathrm{dumbbell}} + \mathrm{LaNi}_5). \tag{3}$$

The chemical potential of the Ni atom in the Ni dumbbell is obtained via

$$\mu_{\mathrm{Ni}} = \tfrac{1}{7}\Big(E(N_{\mathrm{La}} - 1, N_{\mathrm{Ni}} + 2, \mathrm{Ni}_{\mathrm{dumbbell}}) - E(N_{\mathrm{La}}, N_{\mathrm{Ni}}, 0) + \frac{6}{N_{\mathrm{La}} + N_{\mathrm{Ni}}} E(N_{\mathrm{La}}, N_{\mathrm{Ni}}, 0) \Big). \tag{4}$$

The energy of $LaNi_5$ is also calculated using a supercell composed of $N_{\mathrm{La}} + N_{\mathrm{Ni}}$ atoms in order to reduce the error arising from the supercell size.

3. Results and discussion

3.1. Heat of formation of $LaNi_{5+x}$

Figure 2 shows the heat of formation of the La–Ni system around $LaNi_5$ as a function of Ni composition. The heat of formation is calculated by subtracting the total energy of metal La and metal Ni from that of the final state. The composition dependence curves of the heat of formation of $LaNi_{5+x}$ were obtained by interpolating the calculated results using the $1 \times 1 \times 2$, $2 \times 2 \times 2$, $2 \times 2 \times 3$ and $2 \times 2 \times 4$ supercells in which the central atom was replaced by a defect. For comparison, not only Ni dumbbells but also Ni antisite atoms were considered as defects compensating the compositional deviation. In the Ni-rich side of $LaNi_5$, the Ni dumbbell in a La site is more stable than the Ni antisite atom. However, the chemical potential of the Ni dumbbell is larger than metal Ni because the heat of formation of $LaNi_5$ including the Ni dumbbells is higher than the tangent line between the heat of formation of the stoichiometric $LaNi_5$ and metal Ni.

The calculated and experimental lattice parameters [14, 15] are plotted as a function of Ni composition in the Ni-rich side in figure 3. The lattice parameters are normalized by those of stoichiometric composition. Regarding the experimental results,

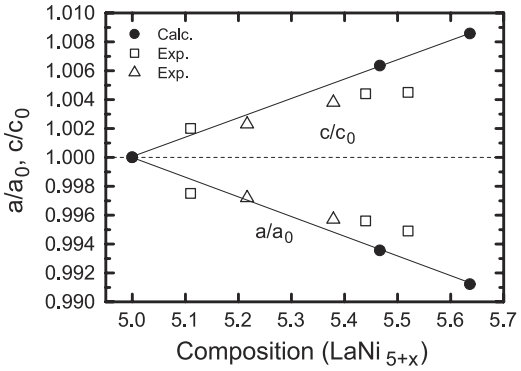

Figure 3. Calculated and experimental lattice parameters as a function of Ni composition in the Ni-rich side of $LaNi_5$. The lattice parameters are normalized by the equilibrium lattice parameter of the stoichiometric composition. Squares and circles represent the experimental results in [14] and in [15], respectively.

Table 1. Calculated vacancy formation energies (in eV).

Chemical Potential	Ni dumbbell		fcc Ni	
Relaxations	Yes	No	Yes	No
Ni (2c)	0.94	1.09	0.75	0.89
Ni (3g)	1.76	1.82	1.57	1.63
fcc Ni			1.39	

the lattice parameter of the a-axis decreases while that of the c-axis increases with increasing Ni composition. The calculated results of $LaNi_{5+x}$ including the Ni dumbbells are in good agreement with this trend. The change in the lattice parameters arises from structural relaxations around the Ni dumbbell. Figure 4 shows the atomic structure around the Ni dumbbell obtained from the calculated results using the $2 \times 2 \times 4$ supercell, the composition of which is $LaNi_{5.467}$. The interspace of the Ni dumbbell induces the inward relaxation of the neighboring Ni atoms at the 3g sites, which leads to the decrease of the a-axis. The Ni dumbbell also moves the Ni atoms at the 2c sites and the La atoms in the adjacent layers outwards and the c-axis increases.

3.2. Vacancy formation energy

The calculated results for vacancy formation energies are listed in table 1. For comparison the vacancy formation energy of fcc Ni is also listed. In addition, in order to evaluate the influence of the structural relaxations, we also calculated the vacancy formation energies using the unrelaxed supercells. We observe a clear site dependence: whereas the formation energy of the Ni vacancy at the 3g site is comparable to that of fcc Ni, the Ni atom at the 2c site has vacancy formation energy about 0.8 eV lower than that of the Ni atom at the 3g site. Structural relaxations around a defect may markedly reduce defect formation energies [16]. However, regarding the results obtained with the unrelaxed supercells, the vacancy formation energy of the Ni 2c site is also about 0.7 eV lower than that of the Ni 3g site. The structural relaxation does not cause the site dependence of vacancy formation energies in $LaNi_5$.

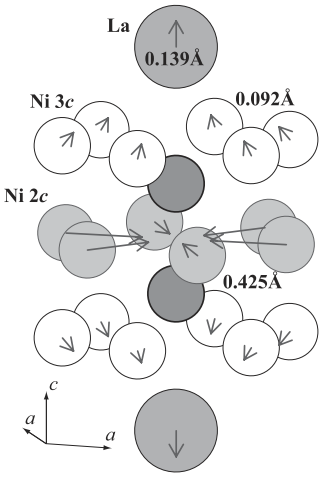

Figure 4. Structures around the Ni dumbbell in the supercell of $La_{15}Ni_{82}$ ($2 \times 2 \times 4$). Arrows with a scale factor of four show the displacements from the ideal position in $LaNi_5$.

Table 2. Bond length and number of bonds at the Ni site in $LaNi_5$ at equilibrium state obtained by the present calculation.

	Bond length (Å)/number of bonds			
	La	Ni (2c)	Ni (3g)	Ni (2c + 3g)
Ni (2c)	2.893/3	2.893/3	2.456/6	2.601/9
Ni (3g)	3.196/4	2.456/4	2.505/4	2.481/8

Figure 5 shows contour plots for the valence electron density in the (001) and (002) planes in $LaNi_5$. The Ni atoms at the 2c sites and the La atoms are located in the (001) plane and the Ni atoms at the 3g sites are in the (002) plane. The bond length of Ni–Ni in the (002) plane, 2.505 Å, is comparable to that of fcc Ni, 2.492 Å. On the other hand, the bond length of Ni–Ni in the (001) plane, 2.893 Å, is 16% longer than that of fcc Ni because the bond lengths of Ni–Ni and La–Ni in the (001) plane are equivalent by symmetry and the atomic radius of La is larger than that of Ni. The electron density of Ni–Ni bonds in the (001) plane is lower than that in the (002) plane, which indicates that the Ni–Ni bond in the (001) plane is weaker than that in the (002) plane. Regarding the average bond lengths for neighboring atoms listed in table 2, the difference in Ni–Ni bond length is reduced because the Ni–Ni bond length in between (001) and (002) planes, 2.456 Å, is shorter than that in the (001) plane. However, the average bond length still shows the same trend: the bond length of the Ni atom at the 2c site is longer than that at the 3g site. The binding energy of the Ni atom at the 2c site is, therefore, weaker than that at the 3g site, which leads to the lower formation energy of the Ni vacancy at the 2c site.

3.3. Change in lattice parameters induced by vacancies

The calculated lattice parameters are plotted as a function of Ni vacancy concentration in figure 6. These results were obtained using the supercell La_8Ni_{39} ($2 \times 2 \times 2$), $La_{12}Ni_{59}$ ($2 \times 2 \times 3$) and $La_{16}Ni_{79}$ ($2 \times 2 \times 4$) including a Ni vacancy at the 2c or 3g site, the compositions of which are $LaNi_{4.875}$, $LaNi_{4.917}$ and $LaNi_{4.938}$, respectively. Regarding the Ni vacancy at the 2c site,

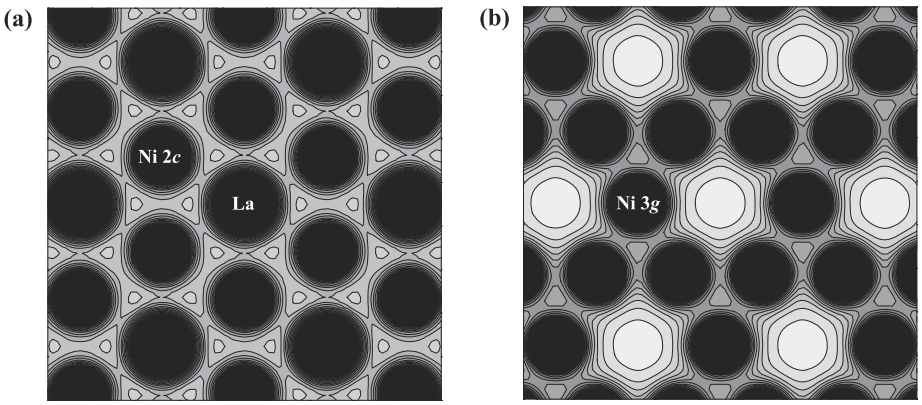

Figure 5. Contour plots of the valence electron density in the plane composed of La and Ni atoms at the 2c sites (a) and composed of Ni atoms at the 3g sites. The interval between contour lines corresponds to 0.00625 electrons $Å^{-3}$.

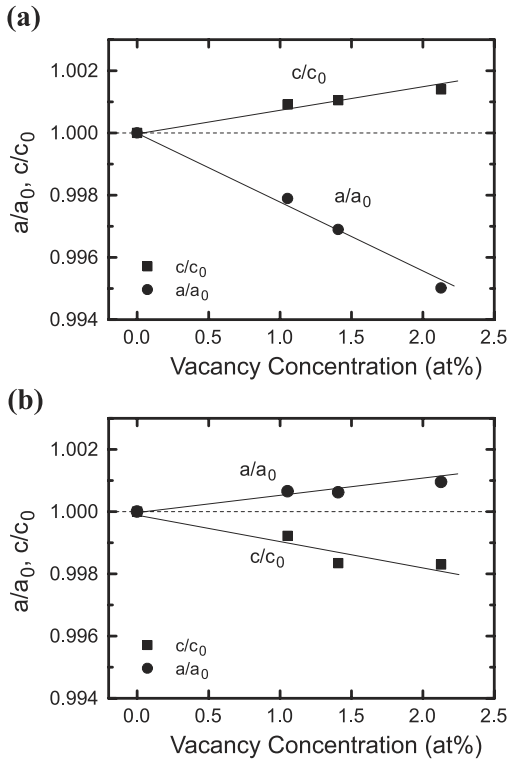

Figure 6. Calculated lattice parameters as a function of concentration of the Ni vacancy at the 2c site (a) and at the 3g site (b). The lattice parameters are normalized by the equilibrium lattice parameter of the stoichiometric composition.

while the lattice parameter of the *a*-axis linearly decreases with increasing vacancy concentration, that of the *c*-axis slightly increases despite accumulation of the vacancies. This is due to the relaxation of the La atoms around the Ni vacancy at the 2c site. Figure 7 shows the atomic structure around the Ni vacancy obtained from the calculated results using the $2 \times 2 \times 4$ supercell. The La atoms around the Ni vacancy at the 2c site relaxed inward towards the Ni vacancy, as seen in figure 7(a). The displaced La atoms restrain inward relaxations of the Ni atoms in the adjacent layers. On the other hand, we see the opposite trend for the Ni vacancy at the 3g sites. This is also

Table 3. Calculated lattice parameters and experimental values before and after activation.

a-axis		*c*-axis		
Unactivated	Activated	Unactivated	Activated	
5.0107	—	3.9690	—	Calc.
5.0228(2)	5.0166(2)	3.9826(2)	3.9846(2)	Exp.[a]
5.0215(1)	5.0141(5)	3.9816(1)	3.9862(3)	Exp.[b]
5.01430(9)	5.0103(4)	3.97987(8)	3.9862(2)	Exp.[c]

[a] Reference [12].
[b] Reference [17].
[c] Reference [18].

due to the relaxation of the La atoms around the Ni vacancy at the 3g site. The La atoms in the adjacent layers relaxed towards the Ni vacancy at the 3g site and displaced the Ni atoms around the Ni vacancy outward, as seen in figure 7(b). The smaller number of neighboring La atoms results in the larger relaxation of La atoms and the large change in the lattice parameters. The arrangement of the La atoms around the Ni vacancy causes the different changes in the lattice parameters.

The experimental lattice parameters of $LaNi_5$ before and after activation (initial hydrogenation) have been reported [12, 17, 18]. The change in lattice parameters after activation is summarized in table 3. These experimental results show similar trends: the lattice parameter of the *a*-axis decrease and that of the *c*-axis increases in the activation process. Compared with our theoretical results, it is suggested that during the hydrogen absorption–desorption process Ni vacancies are mainly formed at the 2c sites, which have a lower formation energy for Ni vacancies than the 3g sites. In order to estimate quantitatively the vacancy concentration, we need to take into account the influence of simultaneously-formed Ni dumbbells, as seen in equation (3), and hydrogen atoms trapped at the vacancies after hydrogen desorption. We will address this problem in the near future.

4. Conclusions

We have investigated vacancy formation in $LaNi_5$ using first-principles calculations. The calculated heat of formation

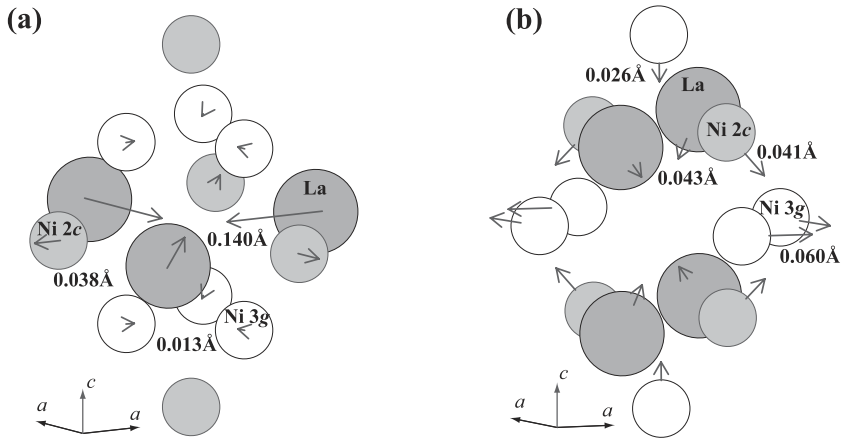

Figure 7. Structures around the Ni vacancy at the 2c site (a) and at the 3g site (b) in the supercell of $La_{16}Ni_{79}$ ($2 \times 2 \times 4$). Arrows with a scale factor of 15 show the displacements induced by vacancy formation.

indicates that Ni dumbbells compensate the deviation from the stoichiometric composition in the Ni-rich side. The calculated lattice parameters including Ni dumbbells agree well with the experimental results in the Ni-rich side. The formation energy of the Ni vacancy at the 2c site is about 0.8 eV lower than that at the 3g site. This is mainly due to the weakness of the Ni–Ni bonding around the Ni atom at the 2c site. The arrangement and relaxation of the La atoms around the Ni vacancy play an important role in changing the lattice parameters induced by the Ni vacancy. In the case of Ni vacancies at the 2c sites, the inward relaxation of neighboring La atoms leads to the decrease of the lattice parameter a and the increase of the lattice parameter c, which shows good agreement with the change in experimental lattice parameters by activation. Both the vacancy formation energies and lattice parameters obtained in the present work indicate that Ni vacancies are mainly formed at the 2c sites by a hydrogen absorption–desorption process in $LaNi_5$.

Acknowledgments

We would like to thank Dr Koji Sakaki (AIST) for many interesting discussions. This work was supported by 'Priority Assistance of the Formation of Worldwide Renowned Centers of Research—The Global COE Program (Project: Center of Excellence for Advanced Structural and Functional Materials Design)' from the Ministry of Education, Culture, Sports, Science and Technology of Japan, and in part by a Grant-in-Aid for Scientific Research from the Ministry of Education, Culture, Sports, Science and Technology of Japan.

References

[1] Shirai Y, Araki H, Mori T, Nakamura W and Sakaki K 2002 *J. Alloys Compounds* **330–332** 125
[2] Sakaki K, Araki H and Shirai Y 2002 *Mater. Trans.* **43** 1494
[3] Mizuno M, Sakaki K, Araki H and Shirai Y 2003 *J. Alloys Compounds* **356/357** 186
[4] Mizuno M, Tonomori R, Sakaki K, Araki H and Shirai Y 2004 *Solid State Ion.* **172** 149
[5] Bowman R C Jr, Luo C H, Ahn C C, Witham C K and Fultz B 1995 *J. Alloys Compounds* **217** 185
[6] Araki H, Date R, Sakaki K, Mizuno M and Shirai Y 2007 *Phys. Status Solidi* c **4** 3510
[7] Kresse G and Furthmuller J 1996 *Comput. Mater. Sci.* **6** 15
[8] Kresse G and Furthmuller J 1996 *Phys. Rev.* B **54** 11169
[9] Perdew J P and Wang Y 1992 *Phys. Rev.* B **45** 13244
[10] Kresse G and Joubert D 1999 *Phys. Rev.* B **59** 1758
[11] Blöchl P E 1994 *Phys. Rev.* B **50** 17953
[12] Thompson P, Reilly J J and Hastings J M 1987 *J. Less-Common Met.* **129** 105
[13] Mayer J, Elsässer C and Fähnle M 1995 *Phys. Status Solidi* b **191** 283
[14] Joubert J-M, Černý R, Latroche M, Leroy E, Guénée L, Percheron-Guégan A and Yvon K 2002 *J. Solid State Chem.* **166** 1
[15] Latroche M, Joubert J-M, Percheron-Guégan A and Bourée-Vigneron F 2004 *J. Solid State Chem.* **177** 1219
[16] Mizuno M, Araki H and Shirai Y 2005 *Mater. Trans.* **46** 1112
[17] Kisi E H, Buckley C E and Gray E M 1992 *J. Alloys Compounds* **185** 369
[18] Nakamura Y, Oguro K, Uehara I and Akiba E 2000 *J. Alloys Compounds* **298** 138